

# Inter-annual variability of the global terrestrial water cycle

Dongqin Yin<sup>1,2</sup>, Michael L. Roderick<sup>1,3</sup>

<sup>1</sup>Research School of Earth Sciences, Australian National University, Canberra, ACT, 2601, Australia

<sup>2</sup>Australian Research Council Centre of Excellence for Climate System Science, Canberra, ACT, 2601, Australia

<sup>3</sup>Australian Research Council Centre of Excellence for Climate Extremes, Canberra, ACT, 2601, Australia

Correspondence to: ([dongqin.yin@anu.edu.au](mailto:dongqin.yin@anu.edu.au))

## Abstract:

1 Variability of the terrestrial water cycle, i.e., precipitation ( $P$ ), evapotranspiration ( $E$ ), runoff ( $Q$ ) and water  
2 storage change ( $\Delta S$ ) is the key to understanding hydro-climate extremes. However, a comprehensive global  
3 assessment for the partitioning of variability in  $P$  between  $E$ ,  $Q$  and  $\Delta S$  is still not available. In this study, we use  
4 the recently released global monthly hydrologic reanalysis product known as the Climate Data Record (CDR) to  
5 conduct an initial investigation of the inter-annual variability of the global terrestrial water cycle. We first  
6 examine global patterns in partitioning the long-term mean  $\bar{P}$  between the various sinks  $\bar{E}$ ,  $\bar{Q}$  and  $\bar{\Delta S}$  and  
7 confirm the well-known patterns with  $\bar{P}$  partitioned between  $\bar{E}$  and  $\bar{Q}$  according to the aridity index. In a new  
8 analysis based on the concept of variability source and sinks we then examine how variability in the  
9 precipitation  $\sigma_P^2$  (the source) is partitioned between the three variability sinks  $\sigma_E^2$ ,  $\sigma_Q^2$  and  $\sigma_{\Delta S}^2$  along with the  
10 three relevant covariance terms, and how that partitioning varies with the aridity index. We find that the  
11 partitioning of inter-annual variability does not simply follow the mean state partitioning. Instead we find that  
12  $\sigma_P^2$  is mostly partitioned between  $\sigma_Q^2$ ,  $\sigma_{\Delta S}^2$  and the associated covariances with limited partitioning to  $\sigma_E^2$ . We also  
13 find that the magnitude of the covariance components can be large and often negative, indicating that variability  
14 in the sinks (e.g.,  $\sigma_Q^2$ ,  $\sigma_{\Delta S}^2$ ) can, and regularly does, exceed variability in the source ( $\sigma_P^2$ ). Further investigations  
15 under extreme conditions revealed that in extremely dry environments the variance partitioning is closely related  
16 to the water storage capacity. With limited storage capacity the partitioning of  $\sigma_P^2$  is mostly to  $\sigma_E^2$ , but as the  
17 storage capacity increases the partitioning of  $\sigma_P^2$  is increasingly shared between  $\sigma_E^2$ ,  $\sigma_{\Delta S}^2$  and the covariance  
18 between those variables. In other environments (i.e., extremely wet and semi-arid/semi-humid) the variance  
19 partitioning proved to be extremely complex and a synthesis has not been developed. We anticipate that a major  
20 scientific effort will be needed to develop a synthesis of hydrologic variability.

## 21 1. Introduction

22

23 In describing the terrestrial branch of the water cycle, the precipitation ( $P$ ) is partitioned into evapotranspiration  
24 ( $E$ ), runoff ( $Q$ ) and change in water storage ( $\Delta S$ ). With averages taken over many years,  $\overline{\Delta S}$  is usually assumed to  
25 be zero and it has long been recognized that the partitioning of the long-term mean annual precipitation ( $\overline{P}$ )  
26 between  $\overline{E}$  and  $\overline{Q}$  was jointly determined by the availability of both water ( $\overline{P}$ ) and energy (represented by the net  
27 radiation expressed as an equivalent depth of water and denoted  $\overline{E}_o$ ). Using data from a large number of  
28 watersheds, Budyko (1974) developed an empirical relation relating the evapotranspiration ratio ( $\overline{E}/\overline{P}$ ) to the  
29 aridity index ( $\overline{E}_o/\overline{P}$ ). The resultant empirical relation and other Budyko-type forms (e.g., Fu, 1981; Choudhury,  
30 1999; Yang et al., 2008, Roderick and Farquhar, 2011; Sposito, 2017) that partition  $P$  between  $E$  and  $Q$  have  
31 proven to be extremely useful in both understanding and characterising the long-term mean annual hydrological  
32 conditions in a given region.

33

34 However, the long-term mean annual hydrologic fluxes rarely occur in any given year. Instead, society must  
35 (routinely) deal with variability around the long-term mean. The classic hydro-climate extremes are droughts and  
36 floods but the key point here is that hydrologic variability is expressed on a full spectrum of time and space scales.  
37 To accommodate that perspective, we need to extend our thinking beyond the long-term mean to ask how the  
38 variability of  $P$  is partitioned into the variability of  $E$ ,  $Q$  and  $\Delta S$  (e.g., Orth and Destouni, 2018).

39

40 Early research on hydrologic variability focussed on extending the Budyko curve. In particular, Koster and Suarez  
41 (1999) used the Budyko curve to investigate inter-annual variability in the water cycle. In their framework, the  
42 evapotranspiration standard deviation ratio (defined as the ratio of standard deviation for  $E$  to  $P$ ,  $\sigma_E/\sigma_P$ ) was (also)  
43 estimated using the aridity index ( $\overline{E}_o/\overline{P}$ ). The classic Koster and Suarez framework has been widely applied and  
44 extended in subsequent investigations of the variability in both  $E$  and  $Q$ , using catchment observations, reanalysis  
45 data and model outputs (e.g., McMahon et al., 2011; Wang and Alimohammadi 2012; Sankarasubramanian and  
46 Vogel, 2002; Zeng and Cai, 2015). However, typical applications of the Koster and Suarez framework have  
47 previously been at regional scales and there is still no comprehensive global assessment for partitioning the  
48 variability of  $P$  into the variability of  $E$ ,  $Q$  and  $\Delta S$ . One reason for the lack of a global comprehensive assessment  
49 is the absence of gridded global hydrologic data. Interestingly, the atmospheric science community have long

50 used a combination of observations and model outputs to construct gridded global-scale atmospheric re-analyses  
51 and such products have become central to atmospheric research. Those atmospheric products also contain  
52 estimates of some of the key water cycle variables (e.g.,  $P$ ,  $E$ ), such as in the widely used interim ECMWF Re-  
53 Analysis (ERA-Interim; Dee et al. 2011). Though efforts have been taken to develop land-based products from  
54 atmospheric reanalyses, e.g., ERA-Land (Balsamo et al., 2013) and MERRA-Land (Reichle et al., 2011) databases,  
55 however, the central aim of atmospheric re-analysis is to estimate atmospheric variables. That atmospheric-centric  
56 aim, understandably, ignores many of the nuances of soil water infiltration, vegetation water uptake, runoff  
57 generation and many other processes of central importance in hydrology.

58

59 Hydrologists have only recently accepted the challenge of developing their own re-analysis type products with  
60 perhaps the first serious hydrologic re-analysis being published as recently as a few years ago (Rodell et al., 2015).  
61 More recently, the Princeton University group has extended this early work by making available a gridded global  
62 terrestrial hydrologic re-analysis product known as the Climate Data Record (CDR) (Zhang et al., 2018). Briefly,  
63 the CDR was constructed by synthesizing multiple in-situ observations, satellite remote sensing products, and  
64 land surface model outputs to provide *gridded* estimates of global land precipitation  $P$ , evapotranspiration  $E$ ,  
65 runoff  $Q$  and total water storage change  $\Delta S$  ( $0.5^\circ \times 0.5^\circ$ , monthly, 1984-2010). In developing the CDR, the authors  
66 adopted local water budget closure as the fundamental hydrologic principle. That approach presented one  
67 important difficulty. Global observations of  $\Delta S$  start with the GRACE satellite mission from 2002. Hence before  
68 2002 there is no direct observational constraint on  $\Delta S$  and the authors made the further assumption that the mean  
69 annual  $\Delta S$  over the full 1984-2010 period was zero at every grid-box. That is incorrect in some regions (e.g.  
70 Scanlon et al., 2018) and represents an observational problem that cannot be overcome. However, our interest is  
71 in the year-to-year variability and for that application, the assumption of no change in the mean annual  $\Delta S$  over  
72 the full 1984-2010 period is unlikely to lead to major problems since we are not looking for subtle changes over  
73 time. With that caveat in mind, the aim of this study is to use this new 27-year gridded hydrologic re-analysis  
74 product to conduct an initial investigation of the inter-annual variability of the terrestrial branch of the global  
75 water cycle.

76

77 The paper is structured as follows. We begin in Section 2 by describing the various climate and hydrologic  
78 databases used in this study, and also include a further assessment of the suitability of the CDR database for this

79 initial variability study. In Section 3, we examine relationships between the mean and variability in the four water  
80 cycle variables ( $P$ ,  $E$ ,  $Q$  and  $\Delta S$ ). In Section 4, we first relate the variabilities to the classical aridity index and  
81 then use those results to evaluate the theory of Koster and Suarez (1999). Subsequently we examine how the  
82 variance of  $P$  is partitioned into the variances (and relevant covariances) of  $E$ ,  $Q$  and  $\Delta S$  and undertake an initial  
83 survey that investigates some of the factors controlling the variance partitioning. We conclude the paper with a  
84 discussion summarising what we have learnt about water cycle variability over land by using the CDR database.

85

## 86 2. Methods and Data

### 87 2.1 Methods

88 The water balance is defined by,

$$89 \quad P(t) = E(t) + Q(t) + \Delta S(t) \quad (1)$$

90 with  $P$  the precipitation,  $E$  the evapotranspiration,  $Q$  the runoff and  $\Delta S$  the total water storage change in time  
91 step  $t$  (annual in this study). By the usual variance law, we have,

$$92 \quad \sigma_P^2 = \sigma_E^2 + \sigma_Q^2 + \sigma_{\Delta S}^2 + 2cov(E, Q) + 2cov(E, \Delta S) + 2cov(Q, \Delta S) \quad (2)$$

93 that includes all relevant variances (denoted  $\sigma^2$ ) and covariances (denoted  $cov$ ). Eq. (2) can be thought of as the  
94 hydrologic variance balance equation.

95

### 96 2.2 Hydrologic and Climatic Data

97

98 We use the Climate Data Record (CDR) database (Zhang et al., 2018) which is a recently released global land  
99 hydrologic re-analysis. This product includes global precipitation  $P$ , evapotranspiration  $E$ , runoff  $Q$  and water  
100 storage change  $\Delta S$  ( $0.5^\circ \times 0.5^\circ$ , monthly, 1984-2010). In this study we focus on the inter-annual variability and  
101 the monthly water cycle variables ( $P$ ,  $E$ ,  $Q$  and  $\Delta S$ ) are aggregated to annual totals. The CDR does not report  
102 additional radiation variables and we use the NASA/GEWEX Surface Radiation Budget (SRB) Release-3.0  
103 (monthly, 1984-2007,  $1^\circ \times 1^\circ$ ) database (Stackhouse et al., 2011) to calculate  $E_o$  (defined as the net radiation  
104 expressed as an equivalent depth of liquid water, Budyko, 1974). We then calculate the aridity index ( $\overline{E_o}/\overline{P}$ ) using  
105  $P$  from the CDR and  $E_o$  from the SRB databases (see Fig. S1a in the Supplementary Material).

106

107 In general, we anticipate two important factors, i.e., the water storage capacity and the presence of ice/snow at the  
108 surface, which are most likely to have influence on the partitioning of hydrologic variability. For the storage, the  
109 active range of the monthly water storage variation was used to approximate the water storage capacity ( $S_{\max}$ ). In  
110 more detail, the water storage  $S(t)$  at each time step  $t$  (monthly here) was first calculated from the accumulation  
111 of  $\Delta S(t)$ , i.e.,  $S(t) = S(t-1) + \Delta S(t)$  where we assumed zero storage at the beginning of the study period (i.e.,  $S(0)$   
112 = 0). With the resulting time series available,  $S_{\max}$  was estimated as the difference between the maximum and  
113 minimum  $S(t)$  during the study period at each grid-box (see Fig. S1b in the Supplementary Material). The  
114 estimated  $S_{\max}$  shows a large range from 0 to 1000 mm with the majority of values from 50 to 600 mm (Fig. S1b),  
115 which generally agrees with global rooting depth estimates assuming that water occupies from 10 to 30% of the  
116 soil volume at field capacity (Jackson et al., 1996; Wang-Erlandsson et al., 2016; Yang et al., 2016). To  
117 characterise snow/ice cover, and to distinguish extremely hot and cold regions, we also make use of a gridded  
118 global land air temperature dataset from the Climatic Research Unit (CRU TS4.01 database, monthly, 1901-2016,  
119  $0.5^\circ \times 0.5^\circ$ ) (Harris et al., 2014). (see Fig. S1c in the Supplementary Material).

120

### 121 2.3 Spatial Mask to Define Study Extent

122

123 The CDR database provides an estimate of the uncertainty ( $\pm 1\sigma$ ) for each of the hydrologic variables ( $P$ ,  $E$ ,  $Q$ ,  
124  $\Delta S$ ) in each month. We use those uncertainty estimates to identify and remove regions with high relative  
125 uncertainty in the CDR data. The relative uncertainty is calculated as the ratio of root mean square of the  
126 uncertainty ( $\pm 1\sigma$ ) to the mean annual  $P$ ,  $E$  and  $Q$  at each grid-box following the procedure used by Milly and  
127 Dunne (2002a). Note that the long term mean  $\Delta S$  is zero by construction in the CDR database, and for that reason  
128 we did not use  $\Delta S$  to calculate the relative uncertainty. Grid-boxes with a relative uncertainty (in  $P$ ,  $E$  and  $Q$ ) of  
129 more than 10% are deemed to have high relative uncertainty (Milly and Dunne, 2002a) and were excluded from  
130 the study extent. The excluded grid-boxes were mostly in the Himalayan region, the Sahara Desert and in  
131 Greenland. The final spatial mask is shown in Fig. S2 and this has been applied throughout this study.

132

### 133 2.4 Further Evaluation of CDR Data for Variability Analysis

134

135 In the original work, the CDR database was validated by comparison with independent observations including (i)  
136 mean seasonal cycle of  $Q$  from 26 large basins (see Fig. 8 in Zhang et al., 2018), (ii) mean seasonal cycle of  $\Delta S$

137 from 12 large basins (Fig. 10 in Zhang et al., 2018), (iii) monthly runoff from 165 medium size basins and a  
138 further 862 small basins (Fig. 14 in Zhang et al., 2018), (iv) summer  $E$  from 47 flux towers (Fig. 16 in Zhang et  
139 al., 2018). Those evaluations did not directly address variability in various water cycle elements. With our focus  
140 on the variability we decided to conduct further validations of the CDR database beyond those described in the  
141 original work. In particular, we focussed on further independent assessments of  $E$  and we use monthly (as opposed  
142 to summer) observations of  $E$  from FLUXNET to evaluate the variability in  $E$ . We also compare the  
143 evapotranspiration  $E$  in the CDR with two other gridded global  $E$  products that were not used to develop the CDR  
144 including the LandFluxEval database ( $1^\circ \times 1^\circ$ , monthly, 1989-2005) (Mueller et al., 2013) and the Max Planck  
145 Institute database (MPI,  $0.5^\circ \times 0.5^\circ$ , monthly, 1982-2011) (Jung et al., 2010). The runoff  $Q$  in the CDR is further  
146 compared with the gridded European  $Q$  product E-RUN ( $0.5^\circ \times 0.5^\circ$ , monthly, 1951-2015) (Gudmundsson and  
147 Seneviratne, 2016).

148

149 For the comparison to FLUXNET observations (Baldocchi et al., 2001; Agarwal et al., 2010) we identified 32  
150 flux tower sites (site locations are shown in Fig. S3 and details are shown in Table S1) having at least three years  
151 of continuous (monthly) measurements using the FluxnetLSM R package (v1.0) (Ukkola et al. 2017). The monthly  
152 totals and annual climatology of  $P$  and  $E$  from CDR generally follow FLUXNET observations, with high  
153 correlations and reasonable Root Mean Square Error (Figs. S4-S5, Table S1). Comparison of the point-based  
154 FLUXNET ( $\sim 100$  m – 1 km scale) with the grid-based CDR ( $\sim 50$  km scale) is problematic since the CDR  
155 represents an area that is at least 2500 times larger than the area represented by the individual FLUXNET towers  
156 and we anticipate that the CDR record would be “smoothed” relative to the FLUXNET record. With that in mind,  
157 we chose to compare the ratio of the standard deviation of  $E$  to  $P$  between the CDR and FLUXNET databases and  
158 this normalised comparison of the hydrologic variability proved encouraging (Fig. S6).

159

160 The comparison of  $E$  between the CDR and the LandFluxEval and MPI databases also proved encouraging. We  
161 found that the monthly mean  $E$  from the CDR database is slightly underestimated compared with LandFluxEVAL  
162 database (Fig. S7a), but agrees closely with the MPI database (Fig. S8a). In terms of variability, the standard  
163 deviations of monthly  $E$  from the CDR are in very close agreement with the LandFluxEVAL database (Fig. S7c),  
164 but there is a bias and scaling offset for the comparison with the MPI database particularly for the grid-cells with  
165 low standard deviation of  $E$  (Fig. S8c). The comparison of runoff  $Q$  between the E-RUN and CDR databases show  
166 that the two databases have very similar spatial patterns of both the long-term mean ( $\bar{Q}$ ) and standard deviation

167 ( $\sigma_Q$ ) of the monthly  $Q$  (Fig. S10). The grid-by-grid comparison results are also encouraging, showing slight bias  
168 of both the long-term mean and standard deviation of monthly  $Q$  in the CDR database compared with the E-RUN  
169 database (Fig. S11).

170

171 We concluded that while the CDR database was unlikely to be perfect, it was nevertheless suitable for an initial  
172 exploratory survey of inter-annual variability in the terrestrial branch of the global water cycle.

173

### 174 3. Mean and Variability of Water Cycle Components

#### 175 3.1 Mean Annual $P$ , $E$ , $Q$ and the Budyko Curve

176

177 The global pattern of mean annual  $P$ ,  $E$ ,  $Q$  using the CDR data (1984-2007) is shown in Fig. 1. The mean annual  
178  $P$  ( $\bar{P}$ ) is prominent in tropical regions, southern China, eastern and western North America (Fig. 1a). The  
179 magnitude of mean annual  $E$  ( $\bar{E}$ ) more or less follows the pattern of  $\bar{P}$  in the tropics (Fig. 1b) while the mean  
180 annual  $Q$  ( $\bar{Q}$ ) is particularly prominent in the Amazon, South and Southeast Asia, tropical parts of west Africa  
181 and in some other coastal regions at higher latitudes (Fig. 1c).

182

183 We relate the grid-box level ratio of  $\bar{E}$  to  $\bar{P}$  in the CDR database to the classical Budyko (1974) curve using the  
184 aridity index ( $\bar{E}_o/\bar{P}$ ) (Fig. 2a). As noted previously, in the CDR database,  $\bar{\Delta S}$  is forced to be zero and this enforced  
185 steady state (i.e.,  $\bar{P} = \bar{E} + \bar{Q}$ ) allowed us to also predict the ratio of  $\bar{Q}$  to  $\bar{P}$  using the same Budyko curve (Fig.  
186 2b). The Budyko curves follow the overall pattern in the CDR data, which agrees with previous studies showing  
187 that the aridity index can be used to predict water availability (e.g., Gudmundsson et al., 2016). However, there is  
188 substantial scatter due to, for example, regional variations related to seasonality, water storage change and the  
189 landscape characteristics (Milly, 1994a, b, Padrón et al., 2017). With that caveat in mind, the overall patterns are  
190 as expected with  $\bar{E}$  following  $\bar{P}$  in dry environments ( $\bar{E}_o/\bar{P} > 1.0$ ) while  $\bar{E}$  follows  $\bar{E}_o$  in wet environments  
191 ( $\bar{E}_o/\bar{P} \leq 1.0$ ) (Fig. 2).

192

#### 193 3.2 Inter-annual Variability in $P$ , $E$ , $Q$ and $\Delta S$

194

195 We use the variance balance equation (Eq. 2) to partition the inter-annual  $\sigma_P^2$  into separate components due to  $\sigma_E^2$ ,  
196  $\sigma_Q^2$ ,  $\sigma_{\Delta S}^2$  along with the three covariance components ( $2cov(E, Q)$ ,  $2cov(E, \Delta S)$ ,  $2cov(Q, \Delta S)$ ) (Fig. 3). The

197 spatial pattern of  $\sigma_P^2$  (Fig. 3a) is very similar to that of  $\bar{P}$  (Fig. 1a), which implies that the  $\sigma_P^2$  is positively  
198 correlated with  $\bar{P}$ . In contrast the partitioning of  $\sigma_P^2$  to the various components is very different from the  
199 partitioning of  $\bar{P}$  (cf. Fig. 1 and 3). First we note that while the overall spatial pattern of  $\sigma_E^2$  more or less follows  
200  $\sigma_P^2$ , the overall magnitude of  $\sigma_E^2$  is much smaller than  $\sigma_P^2$  and  $\sigma_Q^2$  in most regions, and in fact  $\sigma_E^2$  is also generally  
201 smaller than  $\sigma_{\Delta S}^2$ . The prominence of  $\sigma_{\Delta S}^2$  (compared to  $\sigma_E^2$ ) surprised us. The three covariance components  
202 ( $cov(E, Q)$ ,  $cov(E, \Delta S)$ ,  $cov(Q, \Delta S)$ ) are also important in some regions. In more detail, the  $cov(E, Q)$  term is  
203 prominent in regions where  $\sigma_Q^2$  is large and is mostly negative in those regions (Fig. 3e), indicating that years with  
204 lower  $E$  are associated with higher  $Q$  and vice-versa. There are also a few regions with prominent positive values  
205 for  $cov(E, Q)$  (e.g., the seasonal hydroclimates of northern Australia) indicating that in those regions, years with  
206 a higher  $E$  are associated with higher  $Q$ . The  $cov(E, \Delta S)$  term (Fig. 3f) has a similar spatial pattern to the  
207  $cov(E, Q)$  term (Fig. 3e) but with a smaller overall magnitude. Finally, the  $cov(Q, \Delta S)$  term shows a more  
208 complex spatial pattern, with both prominent positive and negative values (Fig. 3g) in regions where  $\sigma_Q^2$  (Fig. 3c)  
209 and  $\sigma_{\Delta S}^2$  (Fig. 3d) are both large.

210

211 These results show that the spatial patterns in variability are not simply a reflection of patterns in the long-term  
212 mean state. On the contrary, we find that of the three primary variance terms, the overall magnitude of (inter-  
213 annual)  $\sigma_E^2$  is the smallest implying the least (inter-annual) variability in  $E$ . This is very different from the  
214 conclusions based on spatial patterns in the mean  $P$ ,  $E$  and  $Q$  (see section 3.1). Further, while  $\sigma_Q^2$  more or less  
215 follows  $\sigma_P^2$  as expected, we were surprised by the magnitude of  $\sigma_{\Delta S}^2$  which, in general, substantially exceeds the  
216 magnitude of  $\sigma_E^2$ . Further, the magnitude of the covariance terms can be important, especially in regions with high  
217  $\sigma_Q^2$ . However, unlike the variances, the covariance can be both positive and negative and this introduces additional  
218 complexity. For example, with a negative covariance it is possible for the variance in  $Q$  ( $\sigma_Q^2$ ) to exceed the variance  
219 in  $P$  ( $\sigma_P^2$ ). To examine that in more detail we calculated the equivalent frequency distribution for each of the plots  
220 in Fig. 3. The results (Fig. S9) further emphasise that in general,  $\sigma_E^2$  is the smallest of the variances (Fig. S9b).  
221 We also note that the frequency distributions for the covariances (Fig. S9efg) are not symmetrical. In summary,  
222 it is clear that spatial patterns in the inter-annual variability of the water cycle (Fig. 3) do not simply follow the  
223 spatial patterns for the inter-annual mean (Fig. 1).

224



### 225 3.3 Relation Between Variability and the Mean State for $P$ , $E$ , $Q$

226

227 Differences in the spatial patterns of the mean (Fig. 1) and inter-annual variability (Fig. 3) in the global water  
228 cycle led us to further investigate the relation between the mean and the variability for each separate component.  
229 Here we relate the standard deviation ( $\sigma_P$ ,  $\sigma_E$ ,  $\sigma_Q$ ) instead of the variance to the mean of each water balance flux  
230 (Fig. 4) since the standard deviation has the same physical units as the mean making the results more comparable.  
231 As inferred previously, we find  $\sigma_P$  to be positively correlated with  $\bar{P}$  but with substantial scatter (Fig. 4a). The  
232 same result more or less holds for the relation between  $\sigma_Q$  and  $\bar{Q}$  (Fig. 4c). In contrast the relation between  $\sigma_E$  and  
233  $\bar{E}$  is very different (Fig. 4b). In particular,  $\sigma_E$  is a small fraction of  $\bar{E}$  and this complements the earlier finding (Fig.  
234 4b) that the inter-annual variability for  $E$  is generally smaller than for the other physical variables ( $P$ ,  $Q$  and  $\Delta S$ ).  
235 (The same result was also found using both LandFluxEVAL and MPI databases, see Fig. S12 in the  
236 Supplementary Material.) Importantly, unlike  $P$  and  $Q$ ,  $E$  is constrained by both water and energy availability  
237 (Budyko, 1974) and the limited inter-annual variability in  $E$  presumably reflects limited inter-annual variability  
238 in the available (radiant) energy ( $E_o$ ). This is something that could be investigated in a future study.

239

### 240 4. Relating the Variability of Water Cycle Components to Aridity

241 In the previous section, we investigated spatial patterns of the mean and the variability in the global water cycle.  
242 In this section, we extend that by investigating the partitioning of  $\sigma_P^2$  to the three primary physical terms ( $\sigma_E^2$ ,  $\sigma_Q^2$ ,  
243  $\sigma_{\Delta S}^2$ ) along with the three relevant covariances. For that, we begin by comparing the Koster and Suarez (1999)  
244 theory against the CDR data and then investigate how the partitioning of the variance is related to the aridity index  
245  $\bar{E}_o/\bar{P}$  (see Fig. S1a in the Supplementary Material). Following that, we investigate variance partitioning in relation  
246 to both our estimate of the storage capacity  $S_{\max}$  (see Fig. S1b in the Supplementary Material) as well as the mean  
247 annual air temperature  $\bar{T}_a$  (see Fig. S1c in the Supplementary Material) that we use as a surrogate for snow/ice  
248 cover. We finalise this section by examining the partitioning of variance at three selected study sites that represent  
249 extremely dry/wet, high/low water storage capacity and the hot/cold spectrums.

250

#### 251 4.1 Comparison with the Koster and Suarez (1999) Theory

252

253 We first evaluate the classical empirical curve of Koster and Suarez (1999) by relating ratios  $\sigma_E/\sigma_P$  and  $\sigma_E/\sigma_P$  to  
254 the aridity index (Fig. 5). The ratio  $\sigma_E/\sigma_P$  in the CDR database is generally overestimated by the empirical Koster

255 and Suarez curve, especially in dry environments (e.g.,  $\overline{E_o}/\overline{P} > 3$ ) (Fig. 5a). The inference here is that the Koster  
256 and Suarez theory predicts  $\sigma_E/\sigma_P$  to approach unity in dry environments while the equivalent value in the CDR  
257 data is occasionally unity but is generally smaller. With  $\sigma_E/\sigma_P$  generally overestimated by the Koster and Suarez  
258 theory we expect, and find, that  $\sigma_Q/\sigma_P$  is generally underestimated by the same theory (Fig. 5b). The same  
259 overestimation was found based on the other two independent databases for  $E$  (LandFluxEVAL and MPI) (Fig.  
260 S13). This overestimation is discussed further in section 5.

261

#### 262 4.2 Relating Inter-annual Variability to Aridity

263

264 Here we examine how the fraction of the total variance in precipitation accounted for by the three primary variance  
265 terms along with the three covariance terms varies with the aridity index ( $\overline{E_o}/\overline{P}$ ) (Fig. 6). (Also see Fig. S14 for  
266 the spatial maps.) The ratio  $\sigma_E^2/\sigma_P^2$  is close to zero in extremely wet regions and has an upper limit noted  
267 previously (Fig. 5a) that approaches unity in extremely dry regions (Fig. 6a). The ratio  $\sigma_Q^2/\sigma_P^2$  is close to zero in  
268 extremely dry regions but approaches unity in extremely wet regions but with substantial scatter (Fig. 6b). The  
269 ratio  $\sigma_{\Delta S}^2/\sigma_P^2$  is close to zero in both extremely dry/wet regions (Fig. 6c) and shows the largest range at an  
270 intermediate aridity index ( $\overline{E_o}/\overline{P} \sim 1.0$ ).

271

272 The covariance ratios are all small in extremely dry (e.g.,  $\overline{E_o}/\overline{P} \geq 6.0$ ) environments and generally show the largest  
273 range in semi-arid and semi-humid environments. The peak magnitudes for the three covariance components  
274 consistently occur when  $\overline{E_o}/\overline{P}$  is close to 1.0 which is the threshold often used to separate wet and dry  
275 environments.

276

#### 277 4.3 Further Investigations on the Factors Controlling Partitioning of the Variance

278

279 Results in the previous section demonstrated that spatial variation in the partitioning of  $\sigma_P^2$  into  $\sigma_E^2$ ,  $\sigma_Q^2$ ,  $\sigma_{\Delta S}^2$  and  
280 the three covariance components is complex (Fig. 6). To help further understand inter-annual variability of the  
281 terrestrial water cycle, we conduct further investigations in this section using two factors likely to have a major  
282 influence on the variance partitioning of  $\sigma_P^2$ . The first is the storage capacity  $S_{\max}$  (see Fig. S1b in the  
283 Supplementary Material). The second is the mean annual air temperature  $\overline{T_a}$  (see Fig. S1c in the Supplementary  
284 Material) which is used here as a surrogate for snow/ice presence.

285

#### 286 4.3.1 Relating Inter-annual Variability to Storage Capacity

287

288 We first relate the partitioning of  $\sigma_P^2$  to water storage capacity ( $S_{\max}$ ) by repeating Fig. 6 but instead we use a  
289 logarithmic scale for the x-axis and we distinguish  $S_{\max}$  via the background colour (Fig. 7). To eliminate the  
290 possible overlap of grid-cells in the colouring process, all the grid-cells over land are further separated using  
291 different latitude ranges (as shown in the four columns of Fig. 7), i.e., 90N-60N, 60N-30N, 30N-0 and 0-90S. We  
292 find that  $S_{\max}$  is relatively high in wet environments ( $\overline{E_o}/\overline{P} \leq 1.0$ , Fig. 7a) but shows no obvious relation to the  
293 partitioning of  $\sigma_P^2$ . However, in dry environments ( $\overline{E_o}/\overline{P} > 1.0$ ) the ratio  $\sigma_E^2/\sigma_P^2$  apparently decreases with the  
294 increase of  $S_{\max}$  (Fig. 7a-d). That relation is particularly obvious in extremely dry environments ( $\overline{E_o}/\overline{P} \geq 6.0$ ) at  
295 equatorial latitudes where there is an upper limit of  $\sigma_E^2/\sigma_P^2$  close to 1.0 when  $S_{\max}$  is small (blue grid-cells in Fig.  
296 7c). The interpretation for those extremely dry environments is that when  $S_{\max}$  is small,  $\sigma_P^2$  is almost completely  
297 partitioned into  $\sigma_E^2$  (Fig. 7bc) with the other variance and covariance components close to zero. While for those  
298 same extremely dry environments, as  $S_{\max}$  increases, the partitioning of  $\sigma_P^2$  is shared between  $\sigma_E^2$  and  $\sigma_{\Delta S}^2$  and their  
299 covariance (Fig. 7cks) while  $\sigma_Q^2$  and its covariance components remain close to zero (Fig. 7gow). However, at  
300 polar latitudes in the northern hemisphere (panels in the first and second columns of Fig. 7) there are variations  
301 that could not be easily associated with variations in  $S_{\max}$  which led us to further investigate the role of snow/ice  
302 on the variance partitioning in the following section.

303

#### 304 4.3.2 Relating Inter-annual Variability to Mean Air Temperature

305

306 To understand the potential role of snow/ice in modifying the variance partitioning, we repeat the previous  
307 analysis (Fig. 7) but here we use the mean annual air temperature ( $\overline{T_a}$ ) to colour the grid-cells to (crudely) indicate  
308 the presence of snow/ice (Fig. 8). The results are complex and not easy to simply understand. The most important  
309 difference revealed by this analysis is in the hydrologic partitioning between cold (first column) and hot (third  
310 column) conditions in wet environments ( $\overline{E_o}/\overline{P} \leq 0.5$ ). In particular, when  $\overline{T_a}$  is high,  $\sigma_P^2$  is almost completely  
311 partitioned into  $\sigma_Q^2$  in wet environments (e.g.,  $\overline{E_o}/\overline{P} \leq 0.5$ , Fig. 8g). In contrast, when  $\overline{T_a}$  is low in a wet  
312 environment ( $\overline{E_o}/\overline{P} \leq 0.5$  in first column of Fig. 8), there are substantial variations in the hydrologic partitioning.  
313 That result reinforces the complexity of variance partitioning in the presence of snow/ice.

314

315 4.4 Case Studies

316

317 The previous results (Section 4.3) have demonstrated that the partitioning of  $\sigma_P^2$  is influenced by the water storage  
 318 capacity ( $S_{\max}$ ) in extremely dry environments ( $\overline{E_o}/\overline{P} \geq 6.0$ ) and that the presence of snow/ice is important (as  
 319 indicated by mean air temperature ( $\overline{T_a}$ )) in extremely wet environments ( $\overline{E_o}/\overline{P} \leq 0.5$ ). In this section, we examine,  
 320 in greater detail, several sites to gain deeper understanding of the partitioning of  $\sigma_P^2$ . For that purpose, we selected  
 321 three sites based on extreme values for the three explanatory parameters, i.e.,  $\overline{E_o}/\overline{P}$  (Fig. S1a),  $S_{\max}$  (Fig. S1b) and  
 322  $\overline{T_a}$  (Fig. S1c). The criteria to select three climate sites are as follows, Site 1: dry ( $\overline{E_o}/\overline{P} \geq 6.0$ ) and small  $S_{\max}$  ( $S_{\max}$   
 323  $\approx 0$ ), Site 2: dry ( $\overline{E_o}/\overline{P} \geq 6.0$ ) and relatively large  $S_{\max}$  ( $S_{\max} \gg 0$ ) and Site 3: wet ( $\overline{E_o}/\overline{P} \leq 0.5$ ) and hot ( $\overline{T_a} > 25$   
 324  $^{\circ}\text{C}$ ). For each of the three classes, we use a representative grid-cell (Fig. 9) to show the original time series (Fig.  
 325 10) and the partitioning of the variability (Fig. 11).

326

327 We show the  $P$ ,  $E$ ,  $Q$  and  $\Delta S$  time series along with the relevant variances and covariances in Fig. 10. Starting  
 328 with the two dry sites, at the site with low storage capacity (Site 1), the time series shows that  $E$  closely follows  
 329  $P$  leaving annual  $Q$  and  $\Delta S$  close to zero (Fig. 10a). The variance of  $P$  ( $\sigma_P^2 = 206.9 \text{ mm}^2$ ) is small and almost  
 330 completely partitioned into the variance of  $E$  ( $\sigma_E^2 = 196.9 \text{ mm}^2$ ), leaving very limited variance for  $Q$ ,  $\Delta S$  and all  
 331 three covariance components (Fig. 10b). At the dry site with larger storage capacity (Site 2),  $E$ ,  $Q$  and  $\Delta S$  do not  
 332 simply follow  $P$  (Fig. 10c). As a consequence, the variance of  $P$  ( $\sigma_P^2 = 2798.0 \text{ mm}^2$ ) is shared between  $E$  ( $\sigma_E^2 =$   
 333  $1150.2 \text{ mm}^2$ ),  $\Delta S$  ( $\sigma_{\Delta S}^2 = 800.5 \text{ mm}^2$ ) and their covariance component ( $2cov(E, \Delta S) = 538.4 \text{ mm}^2$ , Fig. 10d).  
 334 Switching now to the remaining wet and hot site (Site 3), we note that  $Q$  closely follows  $P$ , with  $\Delta S$  close to zero  
 335 and  $E$  showing little inter-annual variation (Fig. 10e). The variance of  $P$  ( $\sigma_P^2 = 57374.4 \text{ mm}^2$ ) is relatively large  
 336 and almost completely partitioned into the variance of  $Q$  ( $\sigma_Q^2 = 57296.4 \text{ mm}^2$ ), leaving very limited variance for  
 337  $E$  and  $\Delta S$  and the three covariance components (Fig. 10f). We also examined numerous other sites with similar  
 338 extreme conditions as the three case study sites and found the same basic patterns as reported above.

339

340 To put the data from the three case study sites into a broader variability context we position the site data onto a  
 341 backdrop of original Fig. 6. As noted previously, at Site 1, the ratio  $\sigma_E^2/\sigma_P^2$  is very close to unity (Fig. 11a), and  
 342 under this extreme condition, we have the following approximation,

343 
$$\sigma_P^2 \approx \sigma_E^2 \quad (\text{Site 1, dry and } S_{\max} \approx 0) \quad (3)$$

344 In contrast, for Site 2 with the same aridity index but higher  $S_{\max}$ , we have,

345 
$$\sigma_P^2 \approx \sigma_E^2 + \sigma_{\Delta S}^2 + 2cov(E, \Delta S) \quad (\text{Site 2, dry and } S_{\max} \gg 0) \quad (4)$$

346 Finally, at Site 3, we have,

347 
$$\sigma_P^2 \approx \sigma_Q^2 \quad (\text{Site 3, wet and hot}) \quad (5)$$

348

349 4.5 Synthesis

350

351 The above simple examples demonstrate that aridity  $\overline{E_o}/\overline{P}$ , storage capacity  $S_{\max}$  and to a lesser extent, air  
 352 temperature  $\overline{T_a}$ , all play some role in the partitioning of  $\sigma_P^2$  to the various components. Our synthesis of the results  
 353 for the partitioning of  $\sigma_P^2$  is summarised in Fig. 12. In dry environments with low storage capacity ( $S_{\max} \approx 0$ ) we  
 354 have minimal runoff and expect that  $\sigma_P^2$  is more or less completely partitioned into  $\sigma_E^2$  (Fig. 12a). In those  
 355 environments, (inter-annual) variations in storage  $\sigma_{\Delta S}^2$  play a limited role in setting the overall variability.  
 356 However, in dry environments with larger storage capacity ( $S_{\max} \gg 0$ ),  $\sigma_E^2$  is only a small fraction of  $\sigma_P^2$  (Fig. 12a)  
 357 leaving most of the overall variance in  $\sigma_P^2$  to be partitioned to  $\sigma_{\Delta S}^2$  and the covariance between  $E$  and  $\Delta S$  (Fig.  
 358 12c and Fig. 12e). This emphasises the hydrological importance of water storage capacity in buffering variations  
 359 of the water cycle under dry conditions.

360

361 Under extremely wet conditions, the largest difference in variance partitioning is not due to differences in storage  
 362 capacity but is instead related to differences in mean air temperature. In wet and hot environments, we have  
 363 maximum runoff and find that  $\sigma_P^2$  is more or less completely partitioned into  $\sigma_Q^2$  (Fig. 12b) while the partitioning  
 364 to  $\sigma_E^2$  and  $\sigma_{\Delta S}^2$  is small. However, in wet and cold environments, the variance partitioning shows great complexity  
 365 with  $\sigma_P^2$  being partitioned into all possible components. We suggest that this emphasises the hydrological  
 366 importance of thermal processes (melting/freezing) under extremely cold conditions.

367

368 However, the most complex patterns to interpret are those for semi-arid to semi-humid environments (i.e.,  
 369  $\overline{E_o}/\overline{P} \sim 1.0$ ). Despite a multitude of attempts over an extended period we were unable to develop a simple useful  
 370 synthesis to summarise the partitioning of variability in those environments. We found that the three covariance  
 371 terms all play important roles and we also found that simple environmental gradients (e.g., dry/wet, high/low  
 372 storage capacity, hot/cold) could not easily explain the observed patterns. We anticipate that vegetation related  
 373 processes (e.g., phenology, rooting depth, gas exchange characteristics, disturbance, etc.) may prove to be  
 374 important in explaining hydrologic variability in these biologically productive regions that support most of human

375 population. This result implies that a major scientific effort will be needed to develop a synthesis of the controlling  
376 factors for variability of the water cycle in these environments.

377

## 378 5. Discussion and Conclusions

379

380 Importantly, hydrologists have long been interested in hydrologic variability, but without readily available  
381 databases it has been difficult to quantify water cycle variability. For example, we are not aware of maps showing  
382 global spatial patterns in variance for any terms of the water balance (except for  $P$ ). In this study, we describe an  
383 initial investigation of the inter-annual variability of the terrestrial branch in the global water cycle that uses the  
384 recently released global monthly Climate Data Record (CDR) database for  $P$ ,  $E$ ,  $Q$  and  $\Delta S$ . The CDR is one of  
385 the first dedicated hydrologic reanalysis databases and includes data for a 27-year period. Accordingly, we could  
386 only examine hydrologic variability over this relatively short period. Further, we expect future improvements and  
387 modifications as the hydrologic community seeks to further develop and refine these new reanalysis databases.  
388 With those caveats in mind, we started this analysis by first investigating the partitioning of  $P$  in the water cycle  
389 in terms of long-term mean and then extended that to the inter-annual variability using a theoretical variance  
390 balance equation (Eq. 2). Despite the initial nature of this investigation we have been able to establish some useful  
391 general principles.

392

393 The mean annual  $P$  is mostly partitioned into mean annual  $E$  and  $Q$ , as is well known, and the results using the  
394 CDR were generally consistent with the earlier Budyko framework (Fig. 2). Having established that, the first  
395 general finding is that the spatial pattern in the partitioning of inter-annual variability in the water cycle is not  
396 simply a reflection of the spatial pattern in the partitioning of the long-term mean. In particular, with the variance  
397 calculations, the annual anomalies are squared and hence the storage anomalies do not cancel out like they do  
398 when calculating the mean. With that in mind, we were surprised that the inter-annual variability of water storage  
399 change ( $\sigma_{\Delta S}^2$ ) is typically larger than the inter-annual variability of evapotranspiration ( $\sigma_E^2$ ) (cf. Fig. 3b and 3d).  
400 The consequence is that  $\sigma_{\Delta S}^2$  is more important than  $\sigma_E^2$  for understanding inter-annual variability of global water  
401 cycle. A second important generalisation is that unlike the variance components which are all positive, the three  
402 covariance components in the theory (Eq. 2) can be both positive and negative. We report results here showing  
403 both large positive and negative values for the three covariance terms (Fig. 3efg). This was especially prevalent  
404 in biologically productive regions ( $0.5 < \overline{E_o} / \overline{P} < 1.5$ , Fig. 3eg). When examining the mean state, we are accustomed

405 to think that  $P$  sets a limit to  $E$ ,  $Q$  and  $\Delta S$ , as per the mass balance (Eq. 1). But the same thinking does not extend  
406 to the variance balance since the covariance terms on the right hand side of Eq. 2 can be both large and negative  
407 leading to circumstances where the variability in the sinks ( $\sigma_E^2$ ,  $\sigma_Q^2$ ,  $\sigma_{\Delta S}^2$ ) could actually exceed variability in the  
408 source ( $\sigma_P^2$ ). These general principles of variance partitioning in the water cycle above may vary at different time  
409 scales (e.g., monthly, daily), and we expect more details of the variability partitioning across various temporal  
410 scales to be investigated in future studies.

411

412 Our initial attempt to develop deeper understanding of variance partitioning was based on a series of case studies  
413 located in extreme environments (wet/dry vs hot/cold vs high/low water storage capacity). The results offered  
414 some further insights about hydrologic variability. For example, under extremely dry (water-limited)  
415 environments, with limited storage capacity ( $S_{\max}$ ) we found that  $E$  follows  $P$  and  $\sigma_E^2$  follows  $\sigma_P^2$ , with  $\sigma_Q^2$  and  $\sigma_{\Delta S}^2$   
416 both approaching zero. However, as  $S_{\max}$  increases, the partitioning of  $\sigma_P^2$  progressively shifts to a balance between  
417  $\sigma_E^2$ ,  $\sigma_{\Delta S}^2$  and  $\text{cov}(E, \Delta S)$  (Figs. 10-12). This result explains the overestimation of  $\sigma_E/\sigma_P$  by the empirical theory of  
418 Koster and Suarez (1999) which implicitly assumed no inter-annual change in storage. The Koster and Suarez  
419 empirical theory is perhaps better described as an upper limit that is based on minimal storage capacity, and that  
420 any increase in storage capacity would promote the partitioning of  $\sigma_P^2$  to  $\sigma_{\Delta S}^2$  particularly under dry conditions  
421 (Figs. 10-12).

422

423 In extremely wet/hot environments (i.e., no snow/ice presence) we found  $\sigma_P^2$  to be mostly partitioned to  $\sigma_Q^2$  (with  
424 both  $\sigma_E^2$  and  $\sigma_{\Delta S}^2$  approaching zero, Fig. 10). In contrast, in extremely wet/cold environments, the partitioning of  
425  $\sigma_P^2$  was highly (spatially) variable presumably because of spatial variability in the all-important thermal processes  
426 (freeze/melt).

427

428 The most complex results were found in mesic biologically productive environments ( $0.5 < \overline{E_o}/\overline{P} < 1.5$ ), where all  
429 three covariance terms (Eq. 2) were found to be relatively large and therefore they all played critical roles in the  
430 overall partitioning of variability (Fig. 6). As noted above, in many of these regions, the (absolute) magnitudes of  
431 the covariances were actually larger than the variances of the water balance components  $E$ ,  $Q$  and  $\Delta S$  (e.g., Fig.  
432 3). That result demonstrates that deeper understanding of the process-level interactions that are embedded within

433 each of the three covariance terms (e.g., the role of seasonal vegetation variation) will be needed to develop  
434 process-based understanding of variability in the water cycle in these biologically productive regions ( $0.5 < \overline{E}_o / \overline{P} < 1.5$ ).  
435

436

437 The syntheses of the long-term mean water cycle originated in 1970s (Budyko, 1974), and it took several decades  
438 for those general principles to become widely adopted in the hydrologic community. The hydrologic data needed  
439 to understand hydrologic variability are only now becoming available. With those data we can begin to develop a  
440 process-based understanding of hydrologic variability that can be used for a variety of purposes, e.g., deeper  
441 understanding of hydro-climatic behaviour, hydrologic risk analysis, climate change assessments and hydrologic  
442 sensitivity studies are just a few applications that spring to mind. The initial results presented here show that a  
443 major intellectual effort will be needed to develop a general understanding of hydrologic variability.

444

445

#### 446 **Acknowledgements**

447 This research was supported by the Australian Research Council (CE11E0098, CE170100023), and D.Y. also  
448 acknowledges support by the National Natural Science Foundation of China (51609122). We thank Dr Anna  
449 Ukkola for help in accessing the FLUXNET database. We thank the reviewers (including Dr René Orth and two  
450 anonymous reviewers) for helpful comments that improved the manuscript. The authors declare that there is no  
451 conflict of interests regarding the publication of this paper. All data used in this paper are available online as  
452 referenced in the 'Methods and Data' section.

453

#### 454 **References**

455 Agarwal, D. A., Humphrey, M., Beekwilder, N. F., Jackson, K. R., Goode, M. M., and van Ingen, C.: A data-centered  
456 collaboration portal to support global carbon-flux analysis, *Concurr. Comp-Pract. E.*, 22, 2323-2334,  
457 <https://doi.org/10.1002/cpe.1600>, 2010.

458 Baldocchi, D., Falge, E., Gu, L., Olson, R., Hollinger, D., Running, S., Anthoni, P., Bernhofer, C., Davis, K., Evans, R.,  
459 Fuentes, J., Goldstein, A., Katul, G., Law, B., Lee, X., Malhi, Y., Meyers, T., Munger, W., Oechel, W., Paw U, K. T.,  
460 Pilegaard, K., Schmid, H. P., Valentini, R., Verma, S., Vesala, T., Wilson, K., and Wofsy, S.: FLUXNET: A New Tool  
461 to Study the Temporal and Spatial Variability of Ecosystem-Scale Carbon Dioxide, Water Vapor, and Energy Flux



462 Densities, B. Am. Meteorol. Soc., 82, 2415-2434, [https://doi.org/10.1175/1520-](https://doi.org/10.1175/1520-0477(2001)082<2415:FANTTS>2.3.CO;2)  
463 [0477\(2001\)082<2415:FANTTS>2.3.CO;2](https://doi.org/10.1175/1520-0477(2001)082<2415:FANTTS>2.3.CO;2), 2001.

464 Balsamo, G., Albergel, C., Beljaars, A., Boussetta, S., Brun, E., Cloke, H., Dee, D., Dutra, E., Muñoz-Sabater, J.,  
465 Pappenberger, F., de Rosnay, P., Stockdale, T., and Vitart, F.: ERA-Interim/Land: a global land surface reanalysis  
466 data set, Hydrol. Earth Syst. Sci., 19, 389-407, 10.5194/hess-19-389-2015, 2015.

467 Budyko, M. I.: Climate and Life. Academic Press, London, 1974.

468 Choudhury, B. J.: Evaluation of an empirical equation for annual evaporation using field observations and results  
469 from a biophysical model, J. Hydrol., 216, 99-110, [https://doi.org/10.1016/S0022-1694\(98\)00293-5](https://doi.org/10.1016/S0022-1694(98)00293-5), 1999.

470 Dee, D. P., Uppala, S. M., Simmons, A. J., Berrisford, P., Poli, P., Kobayashi, S., Andrae, U., Balmaseda, M. A.,  
471 Balsamo, G., Bauer, P., Bechtold, P., Beljaars, A. C. M., van de Berg, L., Bidlot, J., Bormann, N., Delsol, C., Dragani,  
472 R., Fuentes, M., Geer, A. J., Haimberger, L., Healy, S. B., Hersbach, H., Hólm, E. V., Isaksen, L., Kållberg, P., Köhler,  
473 M., Matricardi, M., McNally, A. P., Monge-Sanz, B. M., Morcrette, J. J., Park, B. K., Peubey, C., de Rosnay, P.,  
474 Tavolato, C., Thépaut, J. N., and Vitart, F.: The ERA-Interim reanalysis: configuration and performance of the  
475 data assimilation system, Q. J. R. Meteorol. Soc., 137, 553-597, <https://doi.org/10.1002/qj.828>, 2011.

476 Donohue, R. J., Roderick, M. L., and McVicar, T. R.: Can dynamic vegetation information improve the accuracy of  
477 Budyko's hydrological model?, J. Hydrol., 390, 23-34, <https://doi.org/10.1016/j.jhydrol.2010.06.025>, 2010.

478 Fu, B. P.: On the Calculation of the Evaporation from Land Surface, Sci. Atmos. Sin., 5, 23-31, 1981.

479 Gudmundsson, L., Greve, P., and Seneviratne, S. I.: The sensitivity of water availability to changes in the aridity  
480 index and other factors—A probabilistic analysis in the Budyko space, Geophys. Res. Lett., 43, 6985-6994,  
481 <https://doi.org/10.1002/2016GL069763>, 2016.

482 Gudmundsson, L., and Seneviratne, S. I.: Observation-based gridded runoff estimates for Europe (E-RUN version  
483 1.1), Earth Syst. Sci. Data, 8, 279-295, 10.5194/essd-8-279-2016, 2016.

484 Harris, I., Jones, P. D., Osborn, T. J., and Lister, D. H.: Updated high-resolution grids of monthly climatic  
485 observations—the CRU TS3. 10 Dataset, Int. J. Climatol., 34, 623-642, <https://doi.org/10.1002/joc.3711>, 2014.

486 Huning, L. S., and AghaKouchak, A.: Mountain snowpack response to different levels of warming, Proc. Natl.  
487 Acad. Sci. U. S. A., 115, 10932, <https://doi.org/10.1073/pnas.1805953115>, 2018.

488 Jackson, R. B., Canadell, J., Ehleringer, J. R., Mooney, H. A., Sala, O. E., and Schulze, E. D.: A Global Analysis of  
489 Root Distributions for Terrestrial Biomes, Oecologia, 108, 389-411, <https://doi.org/10.1007/BF00333714>, 1996.

490 Jung, M., Reichstein, M., Ciais, P., Seneviratne, S. I., Sheffield, J., Goulden, M. L., Bonan, G., Cescatti, A., Chen, J.,  
491 de Jeu, R., Dolman, A. J., Eugster, W., Gerten, D., Gianelle, D., Gobron, N., Heinke, J., Kimball, J., Law, B. E.,  
492 Montagnani, L., Mu, Q., Mueller, B., Oleson, K., Papale, D., Richardson, A. D., Rouspard, O., Running, S., Tomelleri,  
493 E., Viovy, N., Weber, U., Williams, C., Wood, E., Zaehle, S., and Zhang, K.: Recent decline in the global land  
494 evapotranspiration trend due to limited moisture supply, *Nature*, 467, 951,  
495 <https://doi.org/10.1038/nature09396>, 2010.

496 Koster, R. D., and Suarez, M. J.: A Simple Framework for Examining the Interannual Variability of Land Surface  
497 Moisture Fluxes, *J. Clim.*, 12, 1911-1917, [https://doi.org/10.1175/1520-0442\(1999\)012<1911:ASFFET>2.0.CO;2](https://doi.org/10.1175/1520-0442(1999)012<1911:ASFFET>2.0.CO;2),  
498 1999.

499 McMahon, T. A., Peel, M. C., Pegram, G. G. S., and Smith, I. N.: A Simple Methodology for Estimating Mean and  
500 Variability of Annual Runoff and Reservoir Yield under Present and Future Climates, *J. Hydrometeorol.*, 12, 135-  
501 146, <https://doi.org/10.1175/2010jhm1288.1>, 2011.

502 Milly, P. C. D.: Climate, soil water storage, and the average annual water balance, *Water Resour. Res.*, 30, 2143-  
503 2156, <https://doi.org/10.1029/94WR00586>, 1994a.

504 Milly, P. C. D.: Climate, interseasonal storage of soil water, and the annual water balance, *Adv. Water Resour.*,  
505 17, 19-24, [https://doi.org/10.1016/0309-1708\(94\)90020-5](https://doi.org/10.1016/0309-1708(94)90020-5), 1994b.

506 Milly, P. C. D., and Dunne, K. A.: Macroscale water fluxes 1. Quantifying errors in the estimation of basin mean  
507 precipitation, *Water Resour. Res.*, 38, 23-21-23-14, <https://doi.org/10.1029/2001WR000759>, 2002a.

508 Milly, P. C. D., and Dunne, K. A.: Macroscale water fluxes 2. Water and energy supply control of their interannual  
509 variability, *Water Resour. Res.*, 38, 24-21-24-29, <https://doi.org/10.1029/2001WR000760>, 2002b.

510 Mueller, B., Hirschi, M., Jimenez, C., Ciais, P., Dirmeyer, P. A., Dolman, A. J., Fisher, J. B., Jung, M., Ludwig, F.,  
511 Maignan, F., Miralles, D. G., McCabe, M. F., Reichstein, M., Sheffield, J., Wang, K., Wood, E. F., Zhang, Y., and  
512 Seneviratne, S. I.: Benchmark products for land evapotranspiration: LandFlux-EVAL multi-data set synthesis,  
513 *Hydrol. Earth. Syst. Sci.*, 17, 3707-3720, <https://doi.org/10.5194/hess-17-3707-2013>, 2013.

514 Norby, R. J., Ledford, J., Reilly, C. D., Miller, N. E., and O'Neill, E. G.: Fine-root production dominates response of  
515 a deciduous forest to atmospheric CO<sub>2</sub> enrichment, *Proc. Natl. Acad. Sci. U. S. A.*, 101, 9689-9693,  
516 <https://doi.org/10.1073/pnas.0403491101>, 2004.

517 Orth, R., and Destouni, G.: Drought reduces blue-water fluxes more strongly than green-water fluxes in Europe,  
518 *Nat. Commun.*, 9, 3602, <https://doi.org/10.1038/s41467-018-06013-7>, 2018.

519 Padrón, R. S., Gudmundsson, L., Greve, P., and Seneviratne, S. I.: Large-Scale Controls of the Surface Water  
520 Balance Over Land: Insights From a Systematic Review and Meta-Analysis, *Water Resources Research*, 53, 9659-  
521 9678, [10.1002/2017WR021215](https://doi.org/10.1002/2017WR021215), 2017.

522 Reichle, R. H., Koster, R. D., De Lannoy, G. J. M., Forman, B. A., Liu, Q., Mahanama, S. P. P., and Touré, A.:  
523 Assessment and Enhancement of MERRA Land Surface Hydrology Estimates, *Journal of Climate*, 24, 6322-6338,  
524 [10.1175/JCLI-D-10-05033.1](https://doi.org/10.1175/JCLI-D-10-05033.1), 2011.

525 Rodell, M., Beaudoin, H. K., L'Ecuyer, T. S., Olson, W. S., Famiglietti, J. S., Houser, P. R., Adler, R., Bosilovich, M.  
526 G., Clayson, C. A., Chambers, D., Clark, E., Fetzer, E. J., Gao, X., Gu, G., Hilburn, K., Huffman, G. J., Lettenmaier,  
527 D. P., Liu, W. T., Robertson, F. R., Schlosser, C. A., Sheffield, J., and Wood, E. F.: The Observed State of the Water  
528 Cycle in the Early Twenty-First Century, *J. Clim.*, 28, 8289-8318, <https://doi.org/10.1175/JCLI-D-14-00555.1>,  
529 2015.

530 Roderick, M. L., and Farquhar, G. D.: A simple framework for relating variations in runoff to variations in climatic  
531 conditions and catchment properties, *Water Resour. Res.*, 47, <https://doi.org/10.1029/2010WR009826>, 2011.

532 Sankarasubramanian, A., and Vogel, R. M.: Annual hydroclimatology of the United States, *Water Resour. Res.*,  
533 38, 19-11-19-12, <https://doi.org/10.1029/2001WR000619>, 2002.

534 Scanlon, B. R., Zhang, Z., Save, H., Sun, A. Y., Müller Schmied, H., van Beek, L. P. H., Wiese, D. N., Wada, Y., Long,  
535 D., Reedy, R. C., Longuevergne, L., Döll, P., and Bierkens, M. F. P.: Global models underestimate large decadal  
536 declining and rising water storage trends relative to GRACE satellite data, *Proc. Natl. Acad. Sci. U. S. A.*,  
537 <https://doi.org/10.1073/pnas.1704665115>, 2018.

538 Sposito, G.: Understanding the Budyko Equation, *Water*, 9, <https://doi.org/10.3390/w9040236>, 2017.

539 Stackhouse, P. W., Gupta, S. K., Cox, S. J., Mikovitz, J. C., Zhang, T., and Hinkelman, L. M.: The NASA/GEWEX  
540 Surface Radiation Budget Release 3.0: 24.5-Year Dataset. In: *GEWEX News*, No. 1, 2011.

541 Ukkola, A. M., Haughton, N., De Kauwe, M. G., Abramowitz, G., and Pitman, A. J.: FluxnetLSM R package (v1.0):  
542 a community tool for processing FLUXNET data for use in land surface modelling, *Geosci. Model. Dev.*, 10, 3379-  
543 3390, <https://doi.org/10.5194/gmd-10-3379-2017>, 2017.

544 Wang, D., and Alimohammadi, N.: Responses of annual runoff, evaporation, and storage change to climate  
545 variability at the watershed scale, *Water Resour. Res.*, 48, <https://doi.org/10.1029/2011WR011444>, 2012.

546 Wang-Erlandsson, L., Bastiaanssen, W. G. M., Gao, H., Jägermeyr, J., Senay, G. B., van Dijk, A. I. J. M., Guerschman,  
547 J. P., Keys, P. W., Gordon, L. J., and Savenije, H. H. G.: Global root zone storage capacity from satellite-based  
548 evaporation, *Hydrol. Earth Syst. Sci.*, 20, 1459-1481, <https://doi.org/10.5194/hess-2015-533>, 2016.

549 Yang, H., Yang, D., Lei, Z., and Sun, F.: New analytical derivation of the mean annual water-energy balance  
550 equation, *Water Resour. Res.*, 44, <https://doi.org/10.1029/2007WR006135>, 2008.

551 Yang, Y., Donohue, R. J., and McVicar, T. R.: Global estimation of effective plant rooting depth: Implications for  
552 hydrological modeling, *Water Resour. Res.*, 52, 8260-8276, <https://doi.org/10.1002/2016WR019392>, 2016.

553 Zeng, R., and Cai, X.: Assessing the temporal variance of evapotranspiration considering climate and catchment  
554 storage factors, *Adv. Water Resour.*, 79, 51-60, <https://doi.org/10.1016/j.advwatres.2015.02.008>, 2015.

555 Zhang, L., Potter, N., Hickel, K., Zhang, Y., and Shao, Q.: Water balance modeling over variable time scales based  
556 on the Budyko framework – Model development and testing, *J. Hydrol.*, 360, 117-131,  
557 <https://doi.org/10.1016/j.jhydrol.2008.07.021>, 2008.

558 Zhang, Y., Pan, M., Sheffield, J., Siemann, A. L., Fisher, C. K., Liang, M. L., Beck, H. E., Wanders, N., MacCracken,  
559 R. F., Houser, P. R., Zhou, T., Lettenmaier, D. P., Ma, Y., Pinker, R. T., Bytheway, J., Kummerow, C. D., and Wood,  
560 E. F.: A Climate Data Record (CDR) for the global terrestrial water budget: 1984-2010, *Hydrol. Earth Syst. Sci.*, 22,  
561 241-263, <https://doi.org/10.5194/hess-22-241-2018>, 2018.

562

563

564 **List of Figures:**

565 Figure 1. Mean annual (1984-2010) (a)  $P$ , (b)  $E$  and (c)  $Q$ .

566 Figure 2. Relationship of mean annual (a) evapotranspiration ( $\bar{E}/\bar{P}$ ) and (b) runoff ( $\bar{Q}/\bar{P}$ ) ratios to the aridity  
567 index ( $\bar{E}_o/\bar{P}$ ) from the CDR and SRB databases.

568 Figure 3. Water cycle variances ( $\sigma_P^2, \sigma_E^2, \sigma_Q^2, \sigma_{\Delta S}^2$ ) and covariances ( $cov(E, Q), cov(E, \Delta S), cov(Q, \Delta S)$ ).

569 Figure 4. Relation between inter-annual mean and standard deviation for (a)  $P$ , (b)  $E$  and (c)  $Q$  from the CDR  
570 database.

571 Figure 5. Relationship of inter-annual standard deviation of (a) evapotranspiration ( $\sigma_E/\sigma_P$ ) and (b) runoff ( $\sigma_Q/\sigma_P$ )  
572 ratios to aridity ( $\bar{E}_o/\bar{P}$ ).

573 Figure 6. Relation between water cycle variances-covariances (see Fig. 3b-g) as a fraction of the variance of  $P$   
574 ( $\sigma_P^2$ ) and the aridity index ( $\bar{E}_o/\bar{P}$ ) coloured by density.

575 Figure 7. Relation between water cycle variances-covariances (see Fig. 3b-g) as a fraction of the variance for  $P$   
576 ( $\sigma_P^2$ ) and the aridity index ( $\bar{E}_o/\bar{P}$ ) for grid-cells over different latitude ranges (i.e., 90N-60N, 60N-30N, 30N-0  
577 and 0-90S). The colours relate to the water storage capacity  $S_{\max}$ .

578 Figure 8. Relation between water cycle variances-covariances (see Fig. 3b-g) as a fraction of the variance for  $P$   
579 ( $\sigma_P^2$ ) and the aridity index ( $\bar{E}_o/\bar{P}$ ) for grid-cells over different latitude ranges (i.e., 90N-60N, 60N-30N, 30N-0  
580 and 0-90S). The colours relate to the mean air temperature ( $\bar{T}_a$ ).

581 Figure 9. Locations of three representative grid-cells used as case study sites.

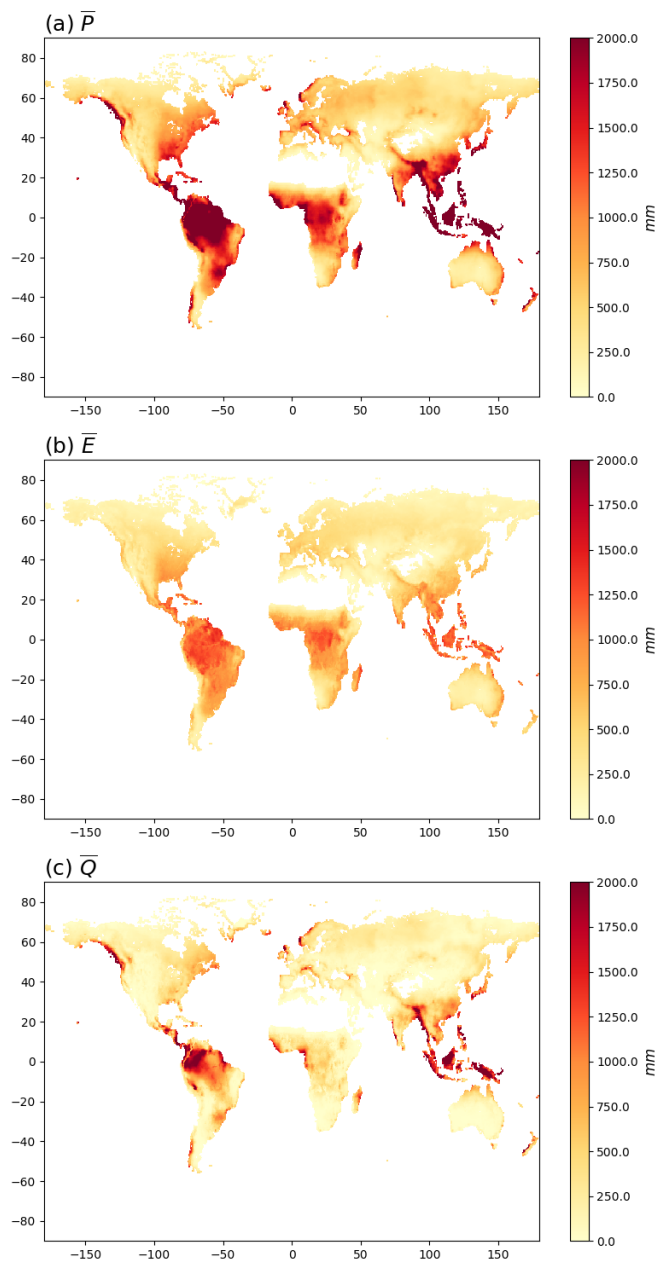
582 Figure 10. Inter-annual time series ( $P, E, Q$  and  $\Delta S$ ) and the associated variance-covariance matrix ( $E, Q$  and  $\Delta S$ )  
583 for case study Sites 1-3.

584 Figure 11. Location of three case study sites in the water cycle variability space.

585 Figure 12. Synthesis of factors controlling variance partitioning.

586

587  
588

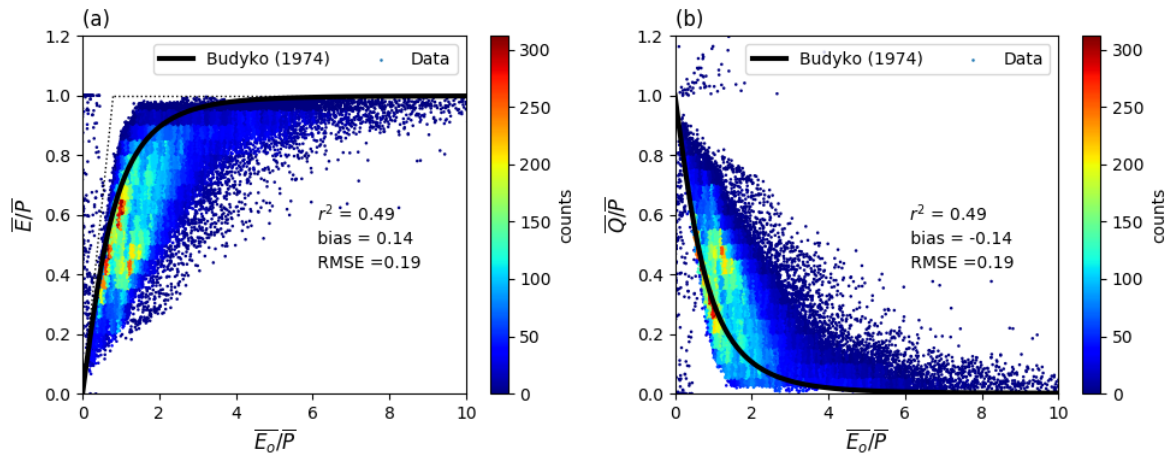


589

590 **Figure 1. Mean annual (1984-2010) (a)  $P$ , (b)  $E$  and (c)  $Q$ . Note that the mean annual  $\Delta S$  in the CDR database is zero**  
591 **by construction and is not shown.**

592

593



594

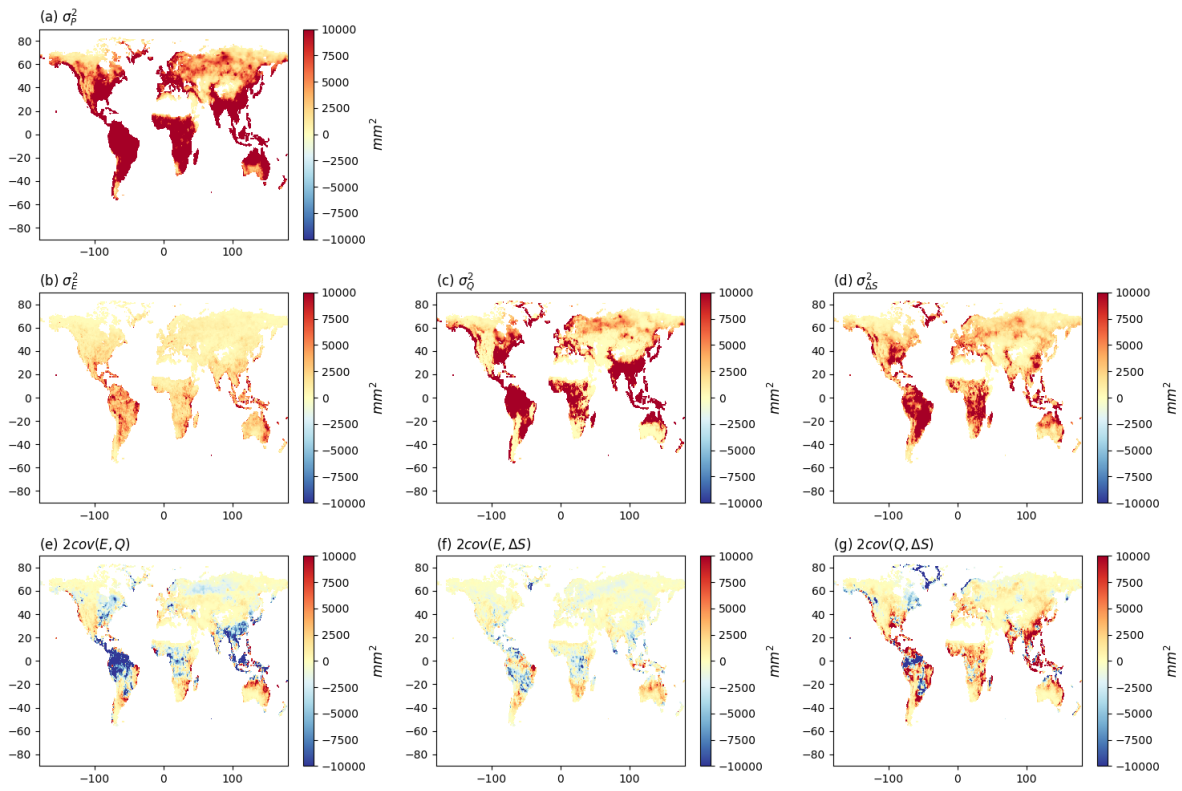
595 **Figure 2. Relationship of mean annual (a) evapotranspiration ( $\bar{E}/\bar{P}$ ) and (b) runoff ( $\bar{Q}/\bar{P}$ ) ratios to the aridity index**

596 **( $\bar{E}_o/\bar{P}$ ) from the CDR and SRB databases. For comparison, the Budyko (1974) curve is shown on the left panel (Fig.**

597 **2a). The curve on the right panel (Fig. 2b) is calculated assuming a steady state ( $\bar{Q}/\bar{P} = 1 - \bar{E}/\bar{P}$ ).**

598

599



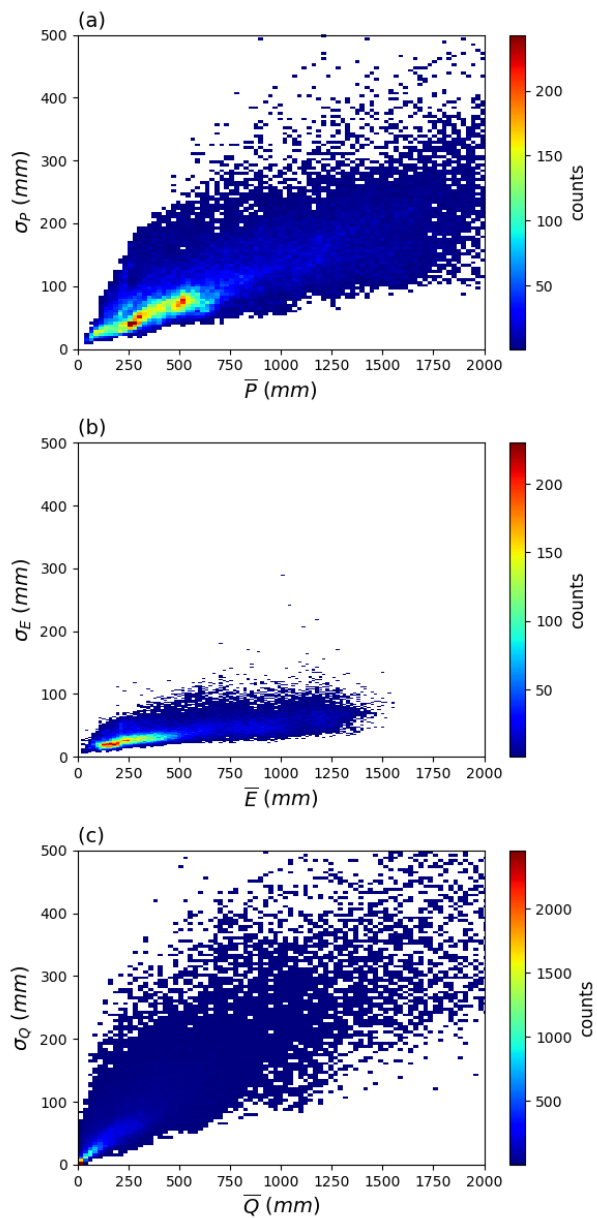
600

601 **Figure 3. Water cycle variances ( $\sigma_p^2, \sigma_E^2, \sigma_Q^2, \sigma_{\Delta S}^2$ ) and covariances ( $cov(E, Q), cov(E, \Delta S), cov(Q, \Delta S)$ ). Note that we**  
602 **have multiplied the covariances by two (see Eq. 2).**

603



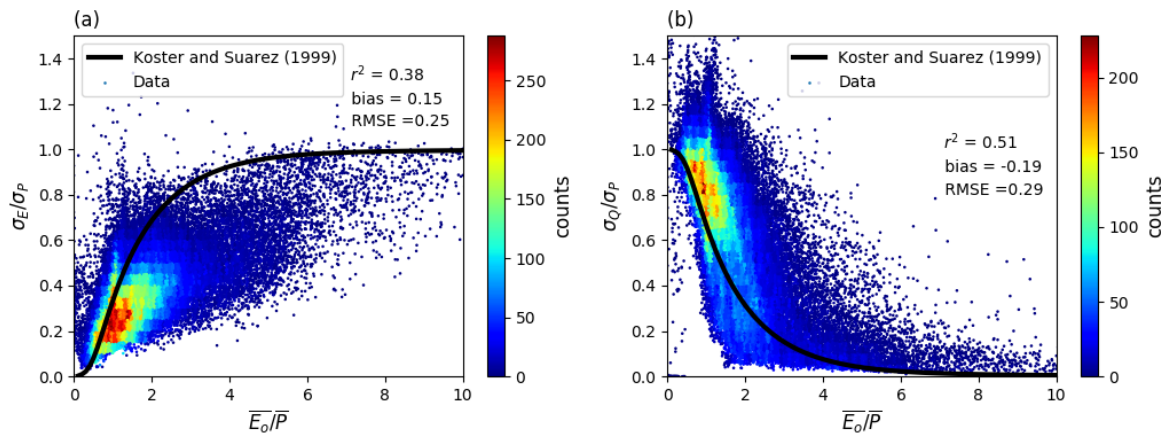
604  
605



606  
607  
608  
609

Figure 4. Relation between inter-annual mean and standard deviation for (a)  $P$ , (b)  $E$  and (c)  $Q$  from the CDR database. Note that the mean annual  $\Delta S$  is zero by construction and is not shown.

610



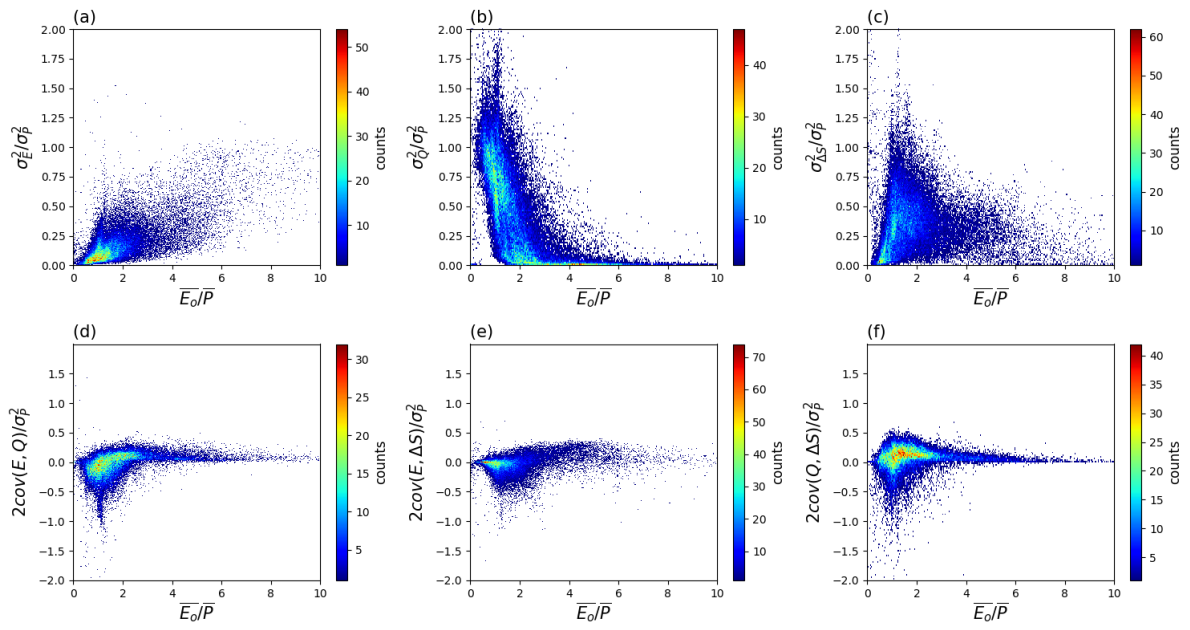
611

612 **Figure 5. Relationship of inter-annual standard deviation of (a) evapotranspiration ( $\sigma_E/\sigma_P$ ) and (b) runoff ( $\sigma_Q/\sigma_P$ )**

613 **ratios to aridity ( $\overline{E_o}/\overline{P}$ ). The curves represent the semi-empirical relations from Koster and Suarez (1999).**

614

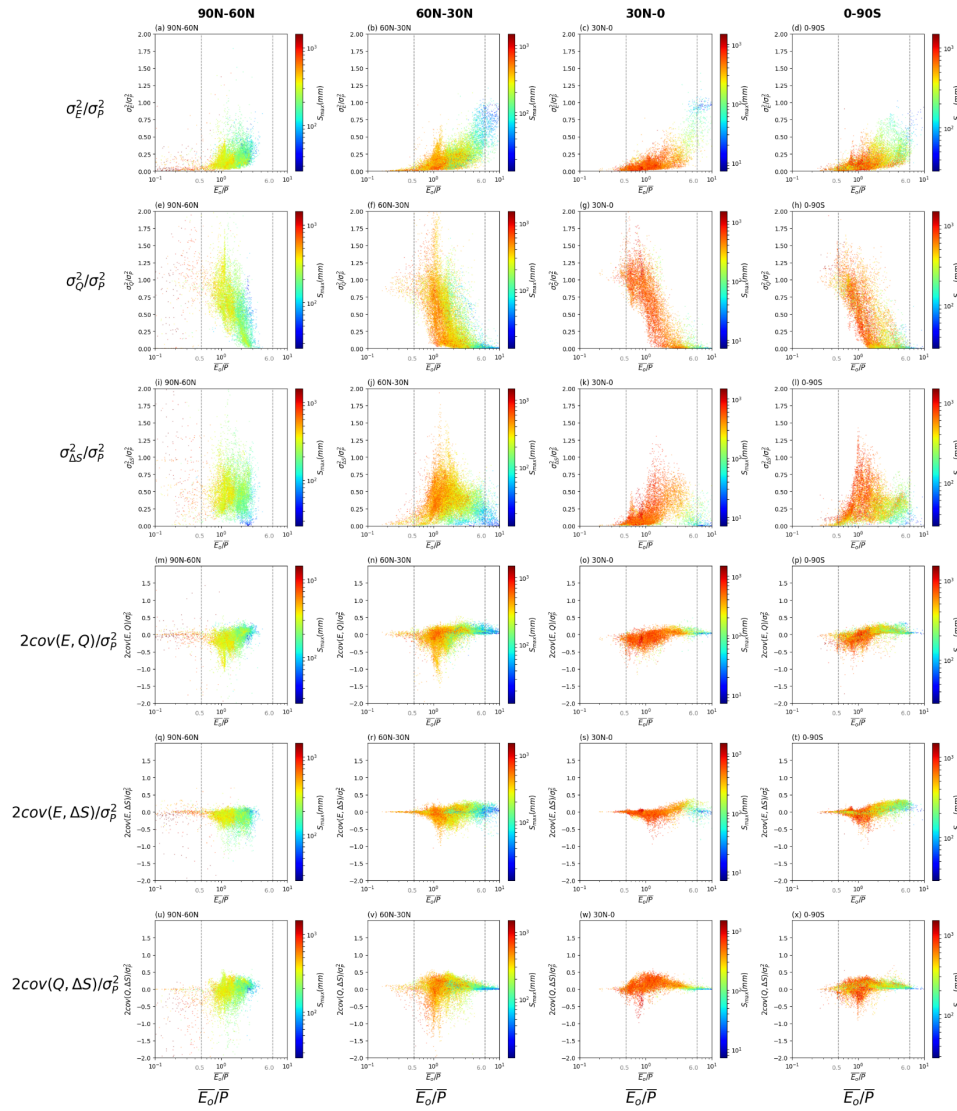
615



616

617 **Figure 6. Relation between water cycle variances-covariances (see Fig. 3b-g) as a fraction of the variance of  $P$  ( $\sigma_P^2$ ) and**  
618 **the aridity index ( $\bar{E}_o/\bar{P}$ ) coloured by density. Note that we have multiplied the covariance components by two (see Eq.**  
619 **2).**

620



622

623 **Figure 7. Relation between water cycle variances-covariances (see Fig. 3b-g) as a fraction of the variance for  $P$  ( $\sigma_P^2$ )**

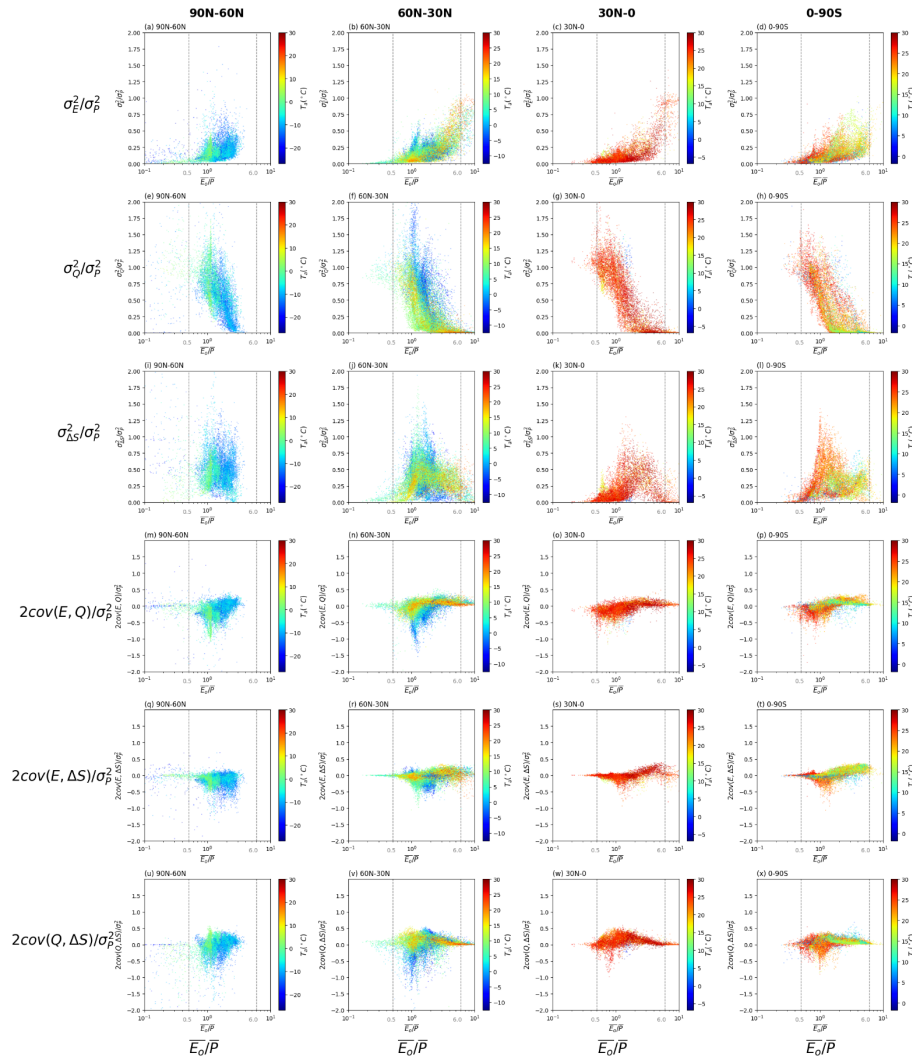
624 **and the aridity index ( $\overline{E_o}/\overline{P}$ ) for grid-cells over different latitude ranges (i.e., 90N-60N, 60N-30N, 30N-0 and 0-90S).**

625 **The colours relate to the water storage capacity  $S_{max}$ . Note that we have multiplied the covariances by two (see Eq. 2).**

626 **The vertical grey dashed lines represent thresholds used to separate extremely dry ( $\overline{E_o}/\overline{P} \geq 6.0$ ) and wet ( $\overline{E_o}/\overline{P} \leq 0.5$ )**

627 **environments. Note the use of a logarithmic x-axis and scale bar for  $S_{max}$ .**

628

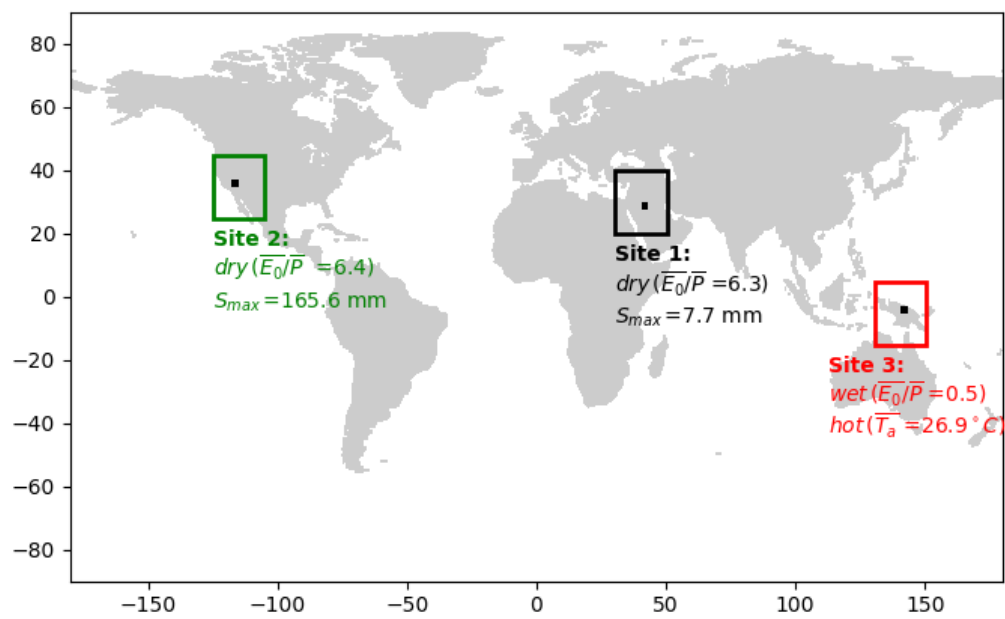


630

631 **Figure 8.** Relation between water cycle variances-covariances (see Fig. 3b-g) as a fraction of the variance for  $P$  ( $\sigma_P^2$ )632 and the aridity index ( $\overline{E_o}/\overline{P}$ ) for grid-cells over different latitude ranges (i.e., 90N-60N, 60N-30N, 30N-0 and 0-90S).633 The colours relate to the mean air temperature ( $\overline{T_a}$ ). Note that we have multiplied the covariances by two (see Eq. 2).634 The vertical grey dashed lines represent thresholds used to separate extremely dry ( $\overline{E_o}/\overline{P} \geq 6.0$ ) and wet ( $\overline{E_o}/\overline{P} \leq$ 635  $0.5$ ) environments.

636

637

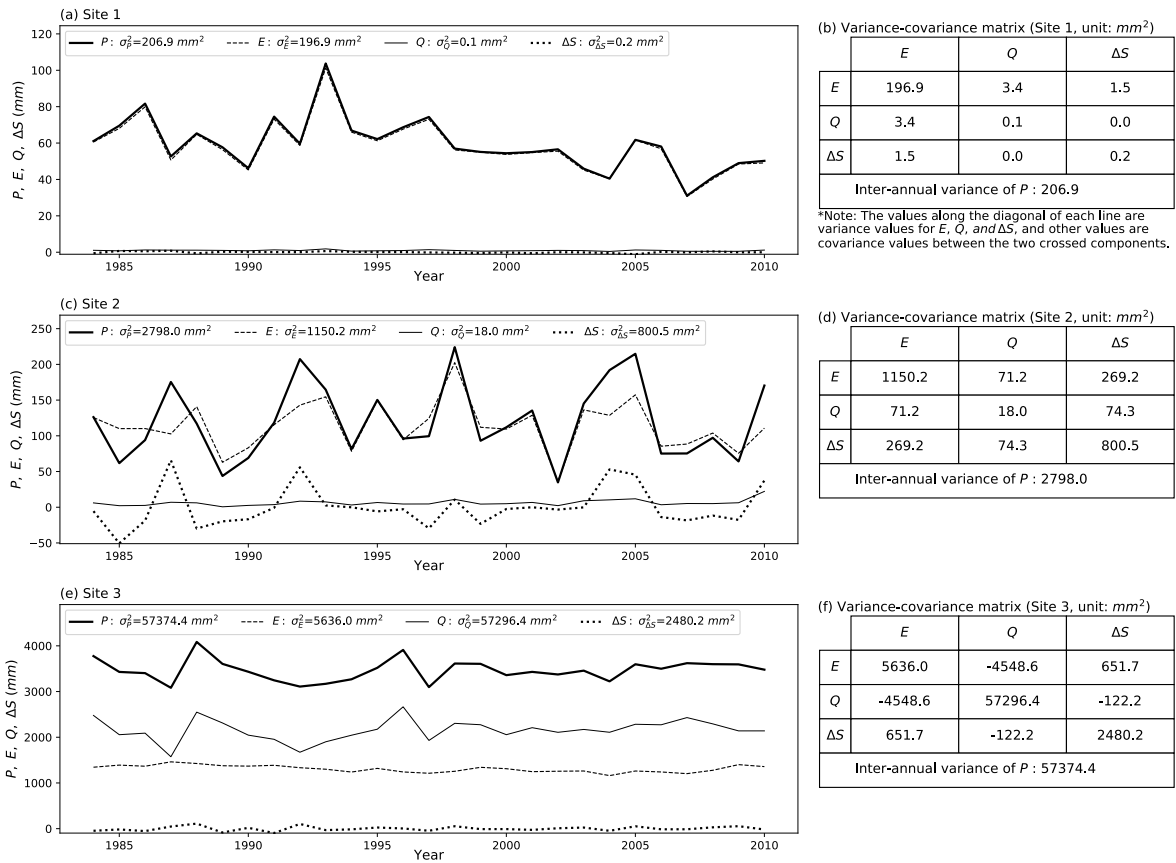


638

639 Figure 9. Locations of three representative grid-cells used as case study sites.

640

641



642

643

644

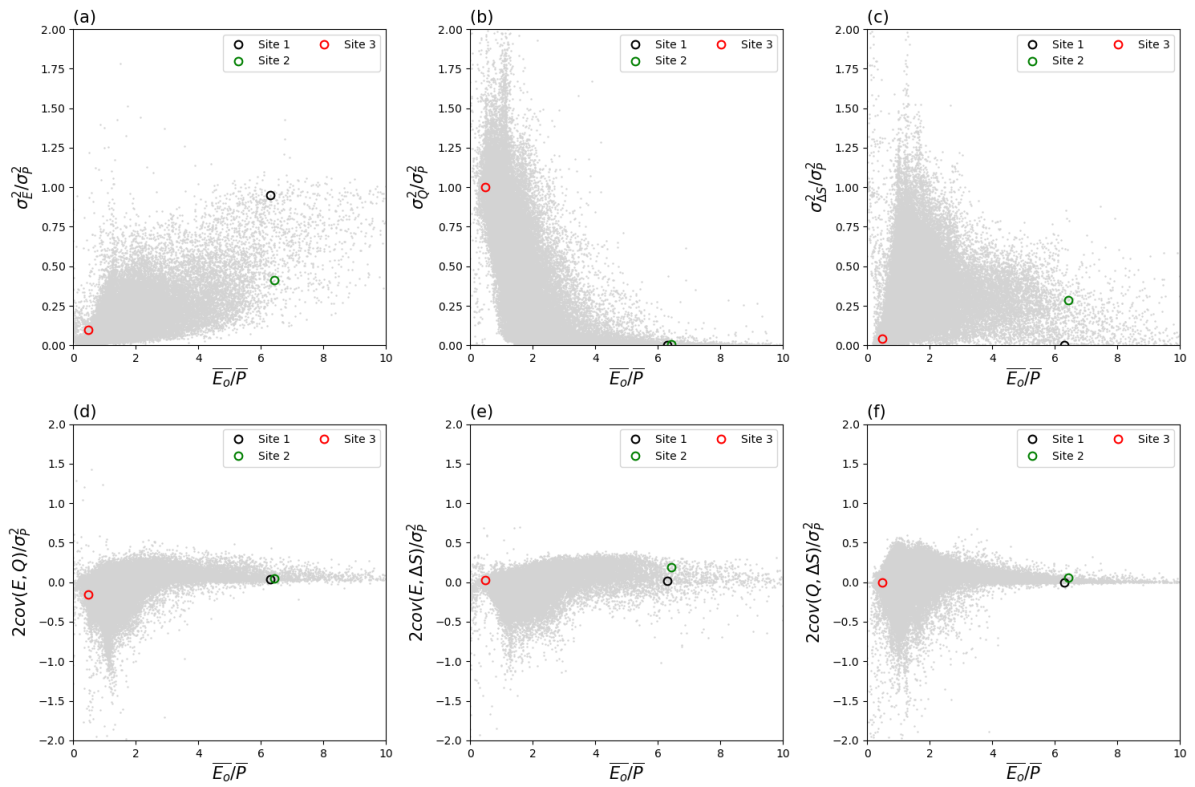
645

646

647

**Figure 10. Inter-annual time series ( $P$ ,  $E$ ,  $Q$  and  $\Delta S$ ) and the associated variance-covariance matrix ( $E$ ,  $Q$  and  $\Delta S$ ) for case study Sites 1-3. Left column shows time series for (a) Site 1, (c) Site 2 and (e) Site 3, with right column i.e., (b), (d) and (f), the associated variance-covariance matrix for three sites. Note that the covariance values in the tables should be multiplied by two to agree with the variance-covariance balance in Eq. (2).**

648



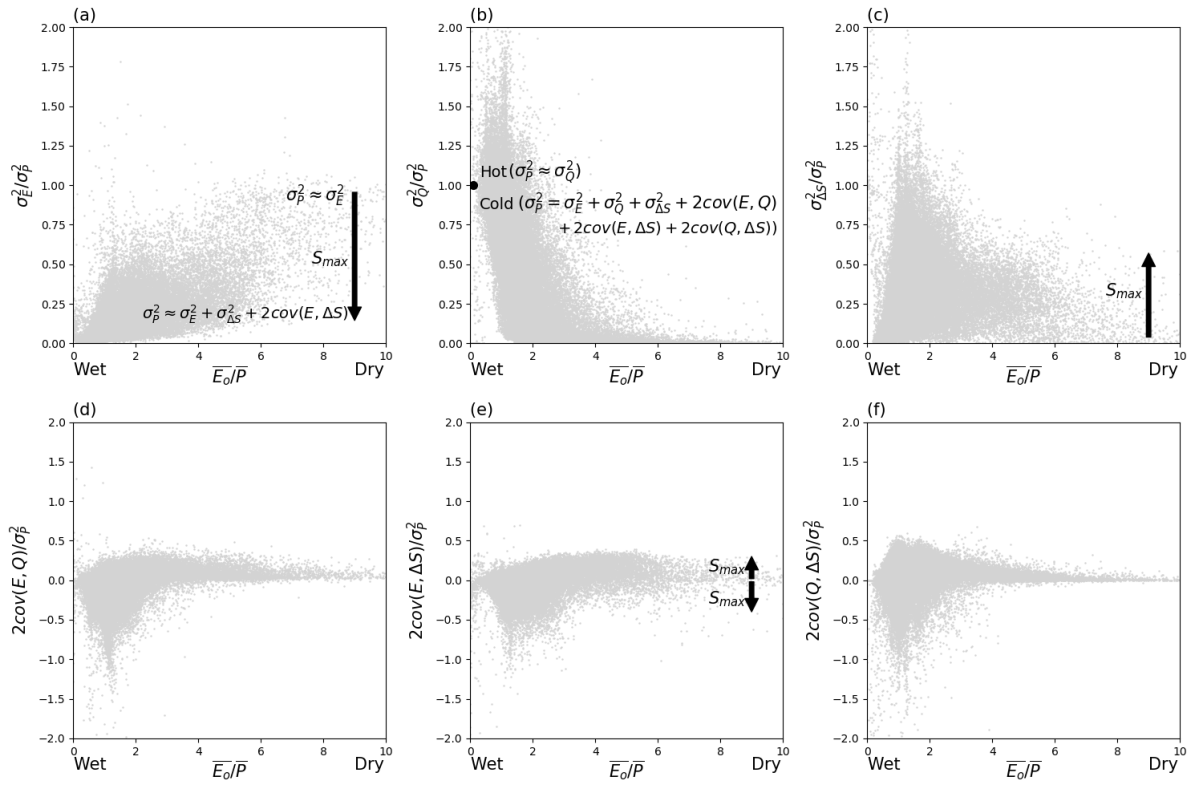
649

650 **Figure 11. Location of three case study sites in the water cycle variability space. The grey background dots are from**  
651 **Fig. 6.**

652



653



654

655 **Figure 12. Synthesis of factors controlling variance partitioning. The arrows denote trends with increasing  $S_{max}$ . The**  
 656 **grey background dots are from Fig. 6.**

657